



OPEN

In vitro model suggests oxidative stress involved in keratoconus disease

SUBJECT AREAS:

MECHANISMS OF
DISEASE

PREDICTIVE MARKERS

D. Karamichos¹, A. E. K. Hutcheon², C. B. Rich⁴, V. Trinkaus-Randall⁴, J. M. Asara³ & J. D. Zieske²

¹Department of Ophthalmology, University of Oklahoma Health Sciences Center, USA, ²Schepens Eye Research Institute/Massachusetts Eye and Ear and the Department of Ophthalmology Harvard Medical School, Boston, MA, USA, ³Division of Signal Transduction/Mass Spectrometry Core, Beth Israel Deaconess Medical Center, Boston, Massachusetts, USA, ⁴Departments of Biochemistry and Ophthalmology, Boston University School of Medicine, 80 E Concord Street, Boston, MA 02118, USA.

Received
3 February 2014

Accepted
20 March 2014

Published
9 April 2014

Correspondence and
requests for materials
should be addressed to
D.K. (dimitrios-
karamichos@ouhsc.
edu)

Keratoconus (KC) affects 1 : 2000 people and is a disorder where cornea thins and assumes a conical shape. Advanced KC requires surgery to maintain vision. The role of oxidative stress in KC remains unclear. We aimed to identify oxidative stress levels between human corneal keratocytes (HCKs), fibroblasts (HCFs) and keratoconus cells (HKCs). Cells were cultured in 2D and 3D systems. Vitamin C (VitC) and TGF- β 3 (T3) were used for 4 weeks to stimulate self-assembled extracellular matrix (ECM). No T3 used as controls. Samples were analyzed using qRT-PCR and metabolomics. qRT-PCR data showed low levels of collagen I and V, as well as keratocan for HKCs, indicating differentiation to a myofibroblast phenotype. Collagen type III, a marker for fibrosis, was up regulated in HKCs. We robustly detected more than 150 metabolites of the targeted 250 by LC-MS/MS per condition and among those metabolites several were related to oxidative stress. Lactate levels, lactate/malate and lactate/pyruvate ratios were elevated in HKCs, while arginine and glutathione/oxidized glutathione ratio were reduced. Similar patterns found in both 2D and 3D. Our data shows that fibroblasts exhibit enhanced oxidative stress compared to keratocytes. Furthermore the HKC cells exhibit the greatest level suggesting they may have a myofibroblast phenotype.

Keratoconus (KC) is a progressive degenerative disease and is a major clinical problem worldwide. KC affects 4 to 600 per 100,000 people and in advanced cases can lead to severe loss of vision. KC affects the cornea structurally, causing it to thin, weaken and protrude into a more conical shape. While KC appears in the teenage years to young adulthood, its rate of progression is generally unpredictable. Currently, the use of contact lenses is used at the early stages of the disease, whereas advanced stages often require surgery, such as corneal transplantation, to maintain or improve vision. Surgeries, however, do not come without complications, which include vascularization of the corneal tissue and rejection of the donor cornea. Corneal collagen crosslinking (CXL) is a new upcoming treatment for keratoconus disease where riboflavin is added to the cornea and is activated by ultraviolet (UV) light^{1,2}. Riboflavin has been shown to increase collagen crosslinking in the cornea and increase its strength leading to less deformation. The pathogenesis of KC is still unclear, however, a variety of factors have been considered, including genetics and cellular mechanisms, as well as oxidative stress^{3–9}. One of the few recognized links to KC disease is the association of individuals with Down syndrome. Approximately, 15% of the individuals with Down syndrome exhibit KC disease^{6,10}. The common gene defect between the two is the superoxide dismutase-1 (SOD1) where it has been proposed as a possible candidate gene for familial KC¹¹. Other gene defects associated with KC disease include VSX1, COL6A1, COL8A1, and MMP9 as reviewed by Nowak and Gajekka¹².

Oxidative stress is an indication of the accumulation of reactive oxygen species (ROS) that may lead to disturbances in the normal redox state of the cell and cause a toxic effect by free radicals and damage all cellular components, including DNA, proteins and lipids. In humans, oxidative stress has been linked to a variety of diseases, such as cancer¹³, Parkinson's disease¹⁴, heart failure¹⁵, and myocardial infarction^{16,17}. In KC, the mRNA levels of antioxidant enzymes have been investigated¹⁸ in KC cornea buttons. The authors concluded that KC corneas undergo oxidative stress and tissue degradation. In agreement with this study, are several others where the antioxidant activities as well as protein levels have been investigated^{19,20}.

Previously, we used a novel 3D model to study KC, which utilizes human keratoconus cells (HKCs) incubated in the presence of a stabilized derivative of Vitamin C (VitC) and TGF- β 3 (T3). Under these conditions the HKCs deposited an extracellular matrix (ECM) that resembles normal stromal ECM²¹. In that study HKCs without T3 secreted an ECM with fibrotic characteristics.

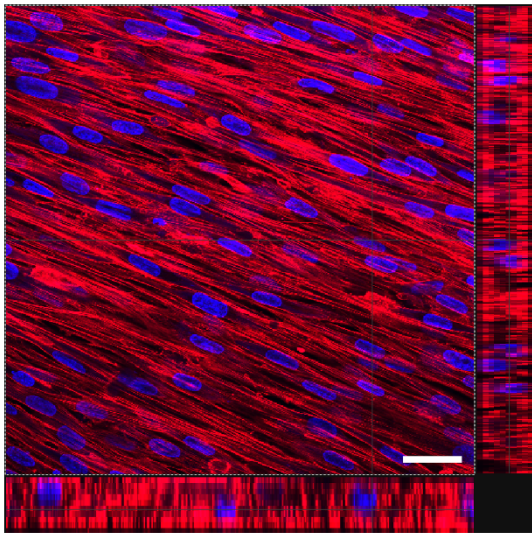


Figure 1 | Representative image showing the morphology of HKCs in 3D cultures. HKCs maintained fibroblastic, elongated morphology under all conditions. Red = Phalloidin, Blue = TOPRO-3. Bars = 50 microns.

Targeted metabolomics using mass spectrometry has been used to profile many diseases such as cancers from biological tissue sources such as cerebral spinal fluid (CSF), plasma and tumor tissue^{22–25}. In our current study, we investigated the metabolic differences between human corneal keratocytes (HCKs), fibroblasts (HCFs) and HKCs, under conventional 2D cultures and using our 3D in vitro model. Investigating both systems allow us to compare cells in a monolayer culture and cells in a self-assembled ECM, which more resembles an in vivo like condition. From these studies, our data indicated that HKCs express metabolites that are indicative of oxidative stress both in the 2D and 3D cultures.

Results

Cell morphology and real time-PCR. We investigated the morphology of the three cell types. Both HKCs and HCFs were elongated or fibroblastic in appearance, while the HKCs were dendritic in shape. Figure 1 shows the morphological phenotype of HKCs which is very similar to HCFs as we have shown previously²⁸. In 3-D cultures, HKCs maintained their dendritic morphology and were distinctively different from HCFs as previously shown²⁸. The morphological characteristics were maintained both with cells in culture and cells on polycarbonate membranes. We did not notice any significant morphological changes between initial cell expansion and experimental conditions.

We further characterized the cells by investigating several essential probes with qRT-PCR for corneal stromal cells: Col I, III and V. Col I and V are routinely found in healthy adult corneal stroma, whereas Col III is a sign of myofibroblast differentiation and a wounded/scarred cornea. We have shown previously²⁸ that Col I and V (~4–5 fold) are significantly upregulated in HKCs and HCFs when T3 is present, independent of VitC stimulation²⁸. In Table 1 we compared the two cell types to HKCs. Expression levels of Col I and Col V, for HKCs, were identical to HCFs; however a 4 fold decrease was seen when compared to HKCs for both Col I and -V. Col III (Table 1) expression was significantly higher (~4 fold) with HKCs when compared to HCFs and even more so when compared to HKCs (~108 fold). Since Col III is a marker for corneal fibrosis and myofibroblast population presence, this is indicative of the different cellular state of the KC corneas. Our data suggest that HKC are myofibroblasts in agreement to previous study where high smooth muscle actin (SMA) expression was shown²¹.

Table 1 | qRT-PCR analysis for all three cell types HKCs, HCFs, and HKCs for Collagen-I, -III and -V. Col I and Col V expression was down-regulated 4 fold in HCFs and HKCs when compared to HKCs. Col III was significantly higher (~4 fold) with HKCs when compared to HCFs and 108 fold compared to HKCs

	Collagen-I (RQ Mean)	Collagen-III (RQ Mean)	Collagen-V (RQ Mean)
HCK	11.46 ± 0.68	0.07667 ± 0.0016	11.43 ± 0.2706
HCF	2.84 ± 0.30	2.27 ± 0.15	1.773 ± 0.1877
HKC	2.763 ± 0.29	8.637 ± 0.61	3.12 ± 0.26

Predicted Pathways of Regulation. Our system allows us to investigate the levels of various metabolites, both in cells that are conventionally cultured (2D), as well as in self-assembled 3D ECM. From our overall raw data analysis, we observed that out of 249 targeted metabolites, the number of those robustly detected ranged from 127 to 155 across the samples with a mean value of 144. In Figure 2 and 3 the predicted metabolic pathways that are affected based on the raw data is shown in 2D (Figure 2) and 3D (Figure 3) systems. When we analyzed the metabolites that were up regulated by at least 2-fold in HKCs compared to HCFs a number of pathways that are involved in oxidative stress were affected. Examples are the citric acid cycle, the glycine-serine-threonine, the betaine and the glutathione metabolism. On the other hand, based on the metabolites where HKCs expressed in higher levels than HKCs, our software indicated significant regulation of pathways that are mainly involved in cell growth (biotin metabolism), toxicity protection (ammonia metabolism, and apoptosis prevention (ubiquinone biosynthesis). Based on these results we further analyzed the metabolites involved in oxidative stress.

Lactate: Cells and Constructs. Our system allows us to investigate the levels of various metabolites, both in cells that are conventionally cultured (2D), as well as in self-assembled 3D ECM. Lactate is produced from pyruvate via glycolysis and is an important metabolite that has been implicated in corneal edema³¹. When lactate levels are high, corneal edema appears. High lactate levels are also a hallmark of many diseases and lactate has become a potential target for cancer therapies³². Figure 4 shows a clear difference in lactate levels between cells cultured in monolayer (2D) and stratified cultures (3D). Lactate levels were significantly ($p < 0.05$) higher when cells were allowed to develop their own ECM and grow in an environment that mimics the in vivo. HKC were significantly higher than both HCFs and HKCs. T3 stimulation only significantly affected HCFs ($p < 0.05$) with a 2 fold up regulation of lactate levels. HKCs showed down regulation of lactate ($p < 0.05$) with the same T3 treatment. Similarly, in the monolayer system, HKCs maintained the lowest levels of lactate when compared to both HCFs and HKCs.

Lactate/Malate ratio: Cells and Constructs. Lactate has been linked to oxidative stress and when paired with other specific metabolites, can act as an indicator of oxidative stress³³. One such combination is the lactate-malate ratio (L/M), which is known to be a critical regulator of oxidative stress^{34,35}. Malate is an intermediate in the citric acid cycle (or TCA cycle) produced from fumarate and an indicator of citric acid cycling. In vivo, the degree of elevation of the ratio and its timing are related to the severity of hypoxia and oxidative stress³⁵. In our systems, HKCs showed the lowest L/M ratio independent of condition and treatment (Figure 5), when compared to both HCFs ($p < 0.05$) and HKCs ($p < 0.01$). In agreement with our lactate data, HKCs seem to be under more oxidative stress. This is enhanced in the 3D system where there is a significant 4 fold difference from the HCF ($p < 0.01$). When HCFs were treated with

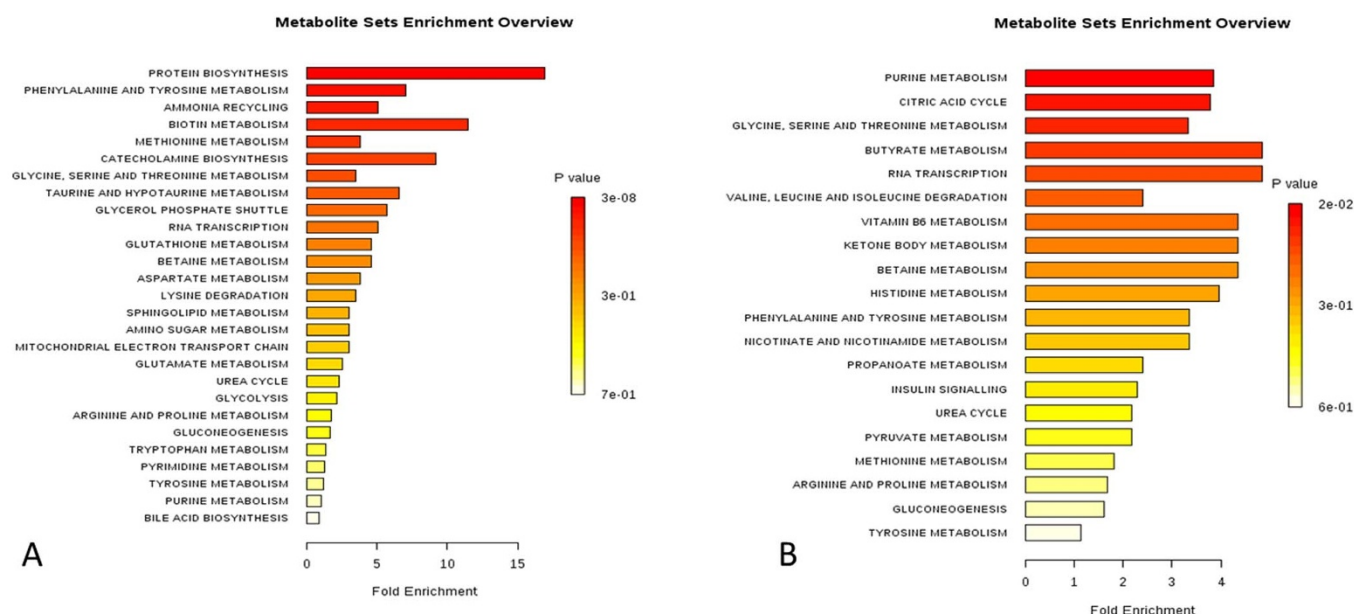


Figure 2 | Summary of pathway enrichment analysis in 2D system. Above is a display of the diversity of signaling pathways that are enriched on the basis of all the metabolites passing filtering criteria. The most significant p-values are in red while the least significant are in yellow and white. A) Shows pathways affected based on metabolites that were at least 2-fold down-regulated in HKCs compared to HCKs, B) Shows pathways affected based on metabolites that were at least 2-fold up-regulated in HKCs compared to HCKs.

T3, L/M ratio was negatively affected showing a 2 and 4 fold up regulation in 2 ($p < 0.05$) and 3D system ($p < 0.01$) respectively. L/M ratio, on the other hand, was reduced in HKCs ($p < 0.05$). Overall, HKCs abnormal levels of oxidative stress are enhanced in the 3D cultures, which is a system more accurately mirroring in vivo regulations (Figure 5). Lactate/malate can indicate the relative levels of glycolytic activity to TCA cycle activity.

Lactate/Pyruvate ratio: Cells and Constructs. Pyruvate represents the final step of glycolysis and a precursor to lactate. The relative ratio

of lactate/pyruvate (L/P) has been used as a measure of anaerobic and aerobic corneal metabolism. However, the ratio also has been proposed as an indicator of oxidative stress²⁸. An increase in the L/P ratio has been reported to accompany corneal degradation and oxidative stress³³. Figure 6 shows ratio regulation on both our systems for all cell types. HCKs showed the lowest ratio of L/P in both systems and all conditions ($p < 0.001$). HKC on the other hand displayed the greatest up regulation of L/P ($p < 0.0001$) in the 3D model indicating oxidative stress. Upon T3 stimulation L/P levels were positively affected and significantly down regulated ($p < 0.001$).

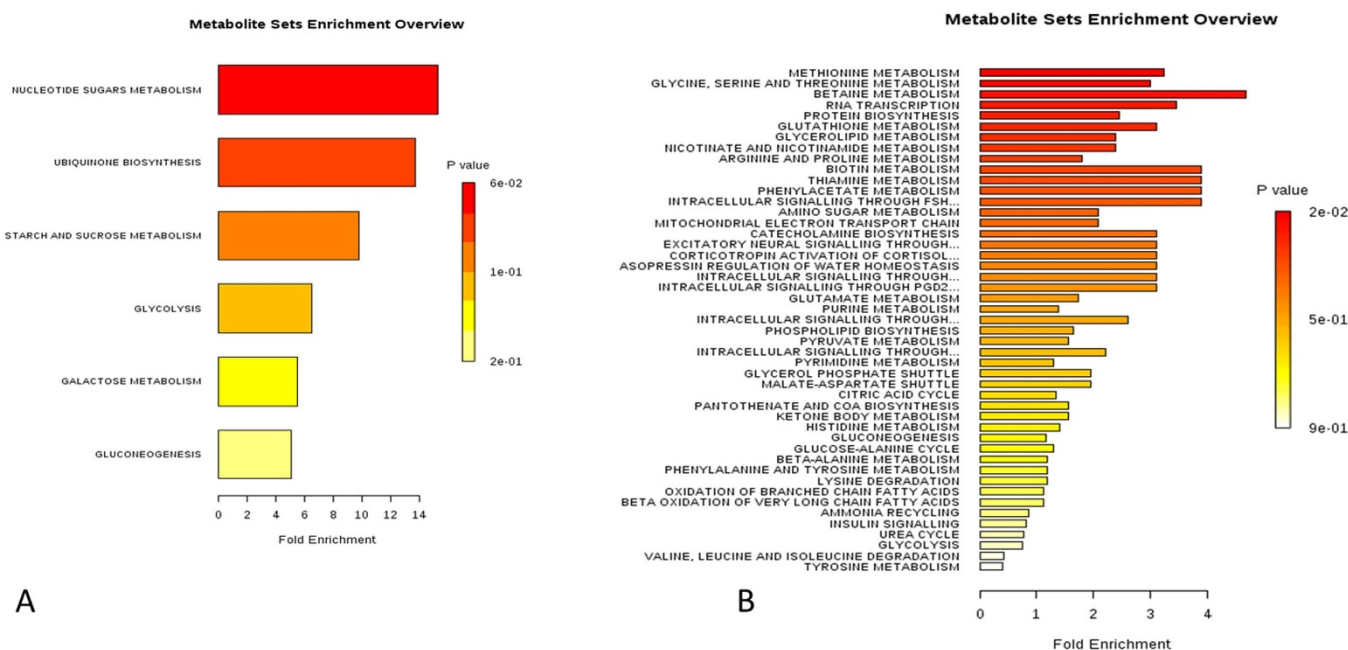


Figure 3 | Summary of pathway enrichment analysis in 3D system. Above is a display of the diversity of signaling pathways that are enriched on the basis of all the metabolites passing filtering criteria. The most significant p-values are in red while the least significant are in yellow and white. A) Shows pathways affected based on metabolites that were at least 2-fold down-regulated in HKCs compared to HCKs, B) Shows pathways affected based on metabolites that were at least 2-fold up-regulated in HKCs compared to HCKs.

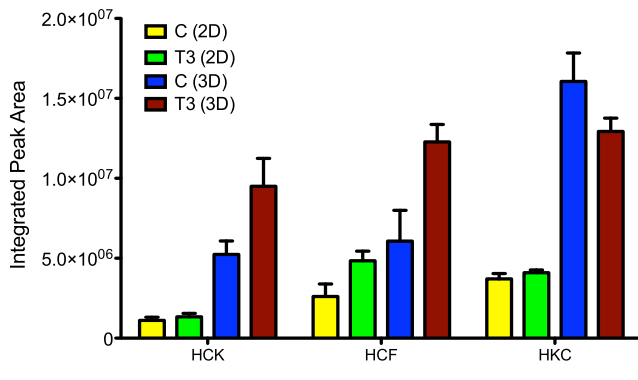


Figure 4 | Lactate metabolite regulation in 2D and 3D culture models for HCKs, HCFs, and HKCs. Two conditions were examined and analyzed for all cell types: Control: VitC only, and T3: VitC + TGF- β 3. Lactate levels were significantly ($p < 0.05$) higher in 3D systems compared to 2D. Upon T3 stimulation only HCFs showed significant up-regulation of Lactate levels ($p < 0.05$).

Consistent with our lactate results, the L/P levels were enhanced in the 3D model for the HKCs. No differences were seen for the HCF which showed identical regulation on all systems and conditions.

GSH ratios: Cells and Constructs. Another way to measure levels of oxidative stress is by looking at a highly studied antioxidant and metabolite glutathione. Glutathione exists in both reduced (GSH) and oxidized (GSSG) states. A decreased GSH-to-GSSG ratio is considered indicative of oxidative stress^{36,37}. In the keratoconic cornea, levels of GSH are low in central corneal buttons³⁸. In this study, we investigated the level of GSH-to-GSSG ratio in our 2D and 3D systems. (Figure 7) The lowest ratio of GSH-to-GSSG was detected in the HKCs ($p < 0.05$) under all systems and conditions, indicating that the cells were and remained under oxidative stress. On the other hand the highest ratio, not surprisingly, was seen with HCKs ($p < 0.05$) indicating less oxidative stress levels. Unlike other indicators so far, such as lactate, L/M and L/P ratios (Figures 4, 5, and 6 respectively), the 3D system seemed to recover some of the HKCs stress levels, i.e. under less oxidative stress. Figure 7 shows higher values of GSH-to-GSSG ratio for all three cell types in the 3D system compared to 2D ($p < 0.05$). T3 treatment significantly increased the ratio values for HCKs ($p < 0.05$) and HCFs ($p < 0.05$), but not for HKCs. Overall, our data throughout showed that HKCs

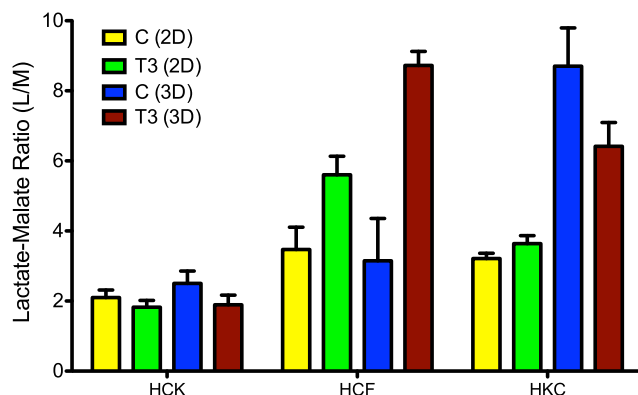


Figure 5 | Lactate to Malate metabolite ratio (L/M) in 2D and 3D culture models for HCKs, HCFs, and HKCs. Two conditions were examined and analyzed for all cell types: Control: VitC only, and T3: VitC + TGF- β 3. HCKs showed the lowest L/M ratio under all conditions compared to both HCFs ($p < 0.05$) and HKCs ($p < 0.01$). T3 significantly increased L/M ratio in HCFs ($p < 0.01$) and decreased it in HKCs ($p < 0.01$).

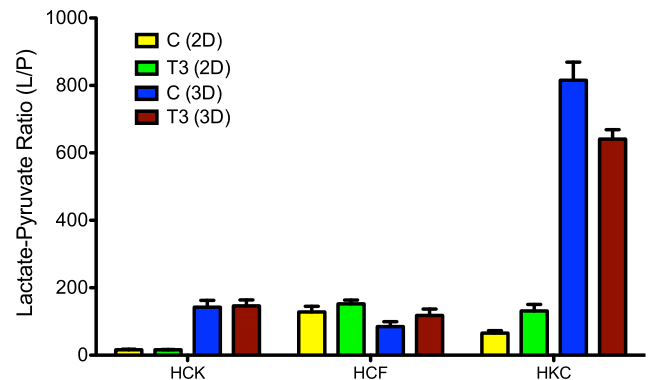


Figure 6 | Lactate to Pyruvate metabolite ratio (L/P) in 2D and 3D culture models for HCKs, HCFs, and HKCs. Two conditions were examined and analyzed for all cell types: Control: VitC only, and T3: VitC + TGF- β 3. HCKs showed the lowest ratio of L/P under all conditions ($p < 0.001$). HKC displayed the greatest up regulation of L/P ($p < 0.0001$) in the 3D model. T3 stimulation reversed that ($p < 0.001$).

are distinct from both HCKs and HCFs and are under more oxidative stress regardless of which system is used (2D or 3D).

Arginine: Cells and Constructs. Arginine is another important metabolite that has been linked to oxidative stress. In the cornea, arginine is a key player in the overall immune privilege of the eye. Inhibition of arginine has been shown to accelerate graft rejection³⁹. We investigated the regulation of arginine in our systems and the results are shown in Figure 8. As expected, HCKs arginine levels were significantly higher than HCFs and HKC ($p < 0.01$), however that was only for the 2D system. In the 3D model, HCKs and HKCs showed similar levels where HCFs were significantly lower. This is another metabolite where its expression is regulated differently when the cells secrete their own ECM versus the conventional cell culture 2D model. While there is a clear indication that HKCs' arginine levels are lower than the native HCKs, and therefore under oxidative stress, our data with T3 is somewhat confusing. In 2D, HCKs showed a massive down regulation of arginine, where HCFs and HKCs did not; where in 3D the effect was inverted with a big up regulation of arginine expression in HCKs. Clearly the role of T3 in oxidative stress regulation is not well understood and further characterization is currently under way.

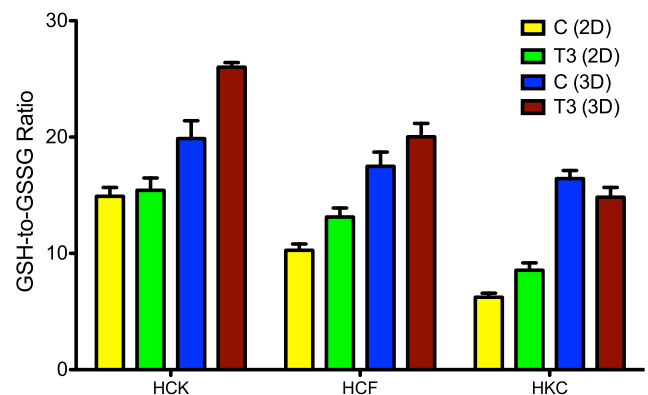


Figure 7 | Glutathione reduced (GSH) to Glutathione oxidized (GSSG) ratio (GSH-to-GSSG) in 2D and 3D culture models for HCKs, HCFs, and HKCs. Two conditions were examined and analyzed for all cell types: Control: VitC only, and T3: VitC + TGF- β 3. HKCs showed the lowest ratio under all conditions ($p < 0.05$). T3 treatment significantly increased the ratio values for HCKs ($p < 0.05$) and HCFs ($p < 0.05$), but not for HKCs.

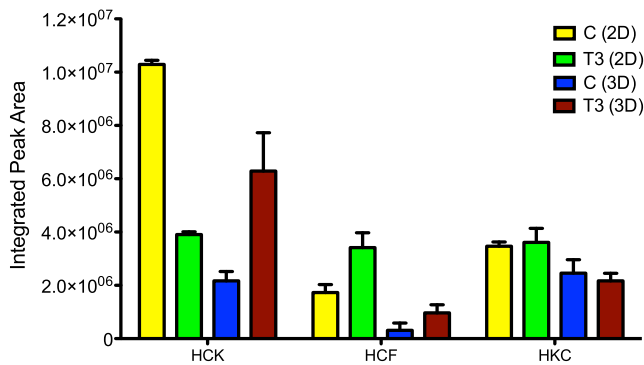


Figure 8 | Arginine metabolite regulation in 2D and 3D culture models for HCKs, HCFs, and HKCs. Two conditions were examined and analyzed for all cell types: Control:VitC only, and T3:VitC + TGF- β 3. HCKs arginine levels were significantly higher than HCFs and HKC ($p < 0.01$) only for the 2D system.

Discussion

Despite the huge advancements in technology, very little is known about metabolic activity of corneal cells derived from Keratoconus patients. This is surprising considering that metabolomics has been used successfully in ocular diseases^{19,20,31,39,40}. We therefore investigated the metabolic activity of corneal cells derived from both normal individual as well as Keratoconus patients. In order to more accurately quantify metabolic activity and correlate it to what is happening in vivo we used two in vitro models; a) conventional 2D cultures and b) a 3D in vitro model that we previously established²⁷ as a novel way to study keratoconus disease at the cellular level in vitro. Our data clearly shows that HKCs are significantly different in terms of their metabolism in vitro, when compared to corneal fibroblasts. Specific metabolites that are known to be key players in oxidative stress were up regulated with HKCs as compared to HCFs indicating oxidative stress status. In turn, both of these cell types were different from normal keratocytes. Almost all metabolites tested here indicated that HCKs were under less stress when compared to either HCFs or HKCs.

Oxidative stress is defined as the imbalance between the systemic manifestation of reactive oxygen species and a biological system's ability to detoxify or repair any resulting damage from the reactive intermediates⁴¹. In humans, oxidative stress depends on the size of these changes and whether the cell can overcome them and return to its original stage. One of the main sources of reactive oxygen is the leakage of activated oxygen from mitochondria during the metabolic pathway of oxidative phosphorylation⁴². The role of the mitochondria in energy metabolism and oxidative stress has been well established^{43–45}. It appears to be intimately linked to their generation of ROS that play a regulatory role in cellular metabolic processes. In fact, the majority of ROS are products of mitochondrial respiration. ROS production and oxidative stress have been linked with an array of pathologies, including type II diabetes, atherosclerosis, ischemia/reperfusion injury, and others^{46–48}.

In ocular surface there have been multiple reports about oxidative stress, including keratoconus. Chwa and co-authors⁴⁹ reported that KC fibroblasts have an inherent, hypersensitive response to oxidative stressors that involves mitochondrial dysfunction and mtDNA damage. Nguyen and co-workers⁴⁰ recently showed that lactate transport was a significant component in the corneal endothelial pump and cornea edema in vivo could be avoided if high levels of lactate were cleared, this was in agreement with previous studies by Klyce³¹. In our system, lactate levels were higher for the Keratoconus cells in the 3D model when compared to Fibroblasts and in both 2D and 3D systems when compared to keratocytes. Fu and coworkers showed that another metabolite, arginine, plays a key role in cornea,

and the overall immune privilege of the eye in vivo³⁹. Arginine inhibition led to accelerated corneal graft rejection. Our data shows that keratocytes had higher level of arginine than both fibroblasts and keratocytes. HCK Control and T3 treated seem to be significantly regulated between the two systems. Taking these together it is clear that Keratoconus cell metabolism is different from normal corneal keratocyte and may provide clues to diagnose and treatment of the disease. Interestingly, both lactate and arginine have been previously linked to corneal edema and thinning^{31,39,40,50} which are characteristics of Keratoconus disease.

Another metabolite that we identified with abnormal levels in the HKCs was glutathione (GSH), an antioxidant peptide that prevents cellular damage from oxidative stress⁵¹. This is in agreement with previous studies showing that GSH contribute to corneal degeneration in keratoconus^{52,53}. In order to ensure accuracy of our results we plotted ratios of GSH with other metabolites that are known to be a sign of oxidative stress such as malate and pyruvate. In all cases HKCs showed such levels suggesting that were under more stress than keratocytes.

The cornea is a transparent avascular tissue that absorbs approximately 80% of the incident ultraviolet B (UVB) light⁵⁴, making it highly sensitive and vulnerable to damage from free radicals and ROS^{54,55}. In the healthy cornea, there are a number of defensive mechanisms that are present to minimize and reduce the risk of oxidative damage^{53,56}. A variety of antioxidant enzymes are present such as catalase, glutathione peroxidase, and glutathione reductase ensuring the removal of ROS generated by UV light exposure⁵⁷. Cells will also defend themselves with enzymes such as alpha-1-microglobulin, superoxide dismutases, glutathione peroxidases and peroxidoxins^{58,59}. Small molecules antioxidants such as Vitamin C, topopherol, and glutathione also play a vital role in the cornea's defense mechanism.

Collectively our data shows that cells derived from Keratoconus patients are under oxidative stress both in conventional 2D model as well as when they secrete their own ECM (ie 3D model). Our pathway prediction software supports this conclusion, as many of the altered pathways in HKCs were oxidative stress related. While this is predictive software it gives us a good indication when alterations between cell types are present. Based on these results future studies should help identify and characterize specific pathways that potentially might lead to metabolic therapies for keratoconus. This is a novel way to study the metabolism of these cells and identify the key players that can help us understand the mechanism behind this disease. Ongoing studies aim to identify more key metabolites as well as further characterize the role of TGF- β 3 in regulating metabolism. Form the data shown here T3 seems to have differential effect on multiple metabolites making its role hard to identify.

Methods

Primary cultures of Human Corneal Keratocytes (HCK), Fibroblasts (HCF) and Keratoconus cells (HKC). HCKs and HCFs were isolated from human corneas from healthy patients without ocular disease. All samples were obtained from NDRI (National Disease Research Interchange; Philadelphia, PA). HKCs were isolated from human corneas from patients with Keratoconus defects. These samples were obtained from Ula Jurkunas (Massachusetts Eye and Ear Infirmary, Boston, MA, USA) and Jesper Hjortdal (Aarhus University Hospital, Aarhus, Denmark). All research adhered to the tenets of the Declaration of Helsinki. Tissue was processed, as previously described²⁶. Briefly, corneal epithelium and endothelium were removed from the stroma by scraping with a razor blade. The stromal tissue was then cut into $\sim 2 \times 2$ mm pieces and placed into T25 culture flasks. Explants were allowed to adhere to the bottom of the wells and then Eagle's Minimum Essential Medium (EMEM; ATCC; Manassas, VA) with either 1% (HCKs) or 10% (HCFs and HKCs) fetal bovine serum (FBS; Atlantic Biologicals; Miami, FL) was added. Following 1–2 weeks of cultivation, the cells were passaged into 100 mm cell culture plates and allowed to grow to 100% confluence before being used in our two systems (2D and 3D).

Conventional 2D cultures. All cell types (HCKs, HCFs and HKCs) were cultured on conventional 6-well tissue culture plates and processed for qRT-PCR. Cells were seeded at 10^6 cells/well and cultured in EMEM with either 1% (HCKs) or 10% FBS



(HCFs and HKCs) + VitC \pm T3 (0.1 ng/ml TGF- β 3: R&D systems, Minneapolis, MN); (Vit C: 0.5 mM 2-O- α -D-glucopyranosyl-L-ascorbic acid: Wako Chemicals USA, Inc.; Richmond, VA). Cultures without T3 served as Controls (C).

Real time PCR (qRT-PCR). Total RNA was extracted and processed, and qRT-PCR was performed, as previously described²¹. Total RNA was extracted from the cells using GeneJet RNA Purification Kit (GeneJet RNA Purification Kit: ThermoScientific, K0731). Genomic DNA was removed by incubation with RNase-free DNase I (New England BioLabs, M0303S) in the presence of RNase inhibitor. The RNA was annealed with oligo dt and random hexamer primers, and first strand synthesis was carried out with MuLV reverse transcriptase (Life technologies, Grand Island, NY). Negative controls were performed without reverse transcriptase. A Vii7A (Life technologies, Grand Island, NY) was used to perform the qRT-PCR with ABI TaqMan gene expression assays—Col1A1: Hs00164004_m1, Col3A1: Hs00943809_m1, Col5A1: Hs00609088_m1, and Keratocan: Hs00559942_m1 and the Eukaryotic 18S rRNA Endogenous Control, 4308329. Results were calculated using the $\Delta\Delta C_t$ method, using 18S rRNA as the endogenous control.

Assembly of Extracellular Matrix – 3D constructs. As previously described^{21,27,28}, cells were plated on transwell 6-well plates containing polycarbonate membrane inserts with 0.4 μ m pores (Costar; Charlotte, NC) at a density of 10^6 cells/ml. Cells were cultured in EMEM with either 1% (HCKs) or 10% FBS (HCFs and HKCs) + VitC \pm T3 (0.1 ng/ml). The cultures were allowed to grow for 4 weeks. The optimal concentration of T3 was previously determined by comparing a concentration series ranging from 0.1–10 ng/ml²⁷. Cultures without T3 served as Controls (C). Constructs thicknesses were similar with our previous studies^{21,27,28}.

Metabolite extraction. All tissues were collected and processed as previously reported^{24,29}. Briefly, samples were grounded using a homogenizer in ice-cold 80% MeOH. Samples were centrifuged (14,000 g, 10 min, 4°C) and supernatants incubated on dry ice. Pellets were further disrupted in ice-cold 80% MeOH and combined with previous supernatants. Plasma metabolites were extracted twice in 80% ice-cold MeOH. Metabolite extracts were vortexed and centrifuged (14,000 g, 10 min, 4°C). Supernatants were evaporated and stored at -80°C until further analysis.

Targeted Mass Spectrometry. Samples were re-suspended using 20 μ L HPLC grade water for mass spectrometry, and 5–7 μ L was injected into a hybrid 5500 QTRAP triple quadrupole mass spectrometer (AB/SCIEX) coupled to a Prominence UFLC HPLC system (Shimadzu, Columbia, MD)^{24,29}. Samples were analyzed via selected reaction monitoring (SRM) of a total of 256 endogenous water soluble metabolites for steady-state analyses. Some metabolites were targeted in both positive and negative ion mode, for a total of 289 SRM transitions, using positive/negative ion polarity switching. ESI voltage was +4900 V in positive ion mode and –4500 V in negative ion mode. The dwell time was 3 ms per SRM transition and the total cycle time was 1.55 seconds. Approximately 10–14 data points were acquired per detected metabolite. Samples were delivered to the mass spectrometer via hydrophilic interaction chromatography (HILIC) using a 4.6 mm i.d \times 10 cm Amide XBridge column (Waters) at 375 μ L/min. Gradients were run as follows: 1) 0–5 minutes with 85 to 42% buffer B (HPLC grade acetonitrile); 2) 5–16 minutes with 42 to 0% buffer B; 3) 16–24 minutes with 0% buffer B; 4) 24–25 minutes with 0 to 85% buffer B; and 5) 7 minutes with 85% buffer B. This last step was to re-equilibrate the column. Peak areas from the total ion current for each metabolite SRM transition were integrated using MultiQuant v2.0 software (AB/SCIEX).

Pathway Enrichment Analysis. Pathway enrichment (representation) analysis was performed using an online freeware program; Metaboanalyst (www.Metaboanalyst.ca) intended for the analysis of metabolomics data.³⁰ Briefly, we performed the analysis using only the metabolites that were up or down regulated by 2-fold as indicated by our statistical analysis. We chose 2-fold cutoff in order to ensure that we included only the vastly abundant metabolites. Only metabolites that were present on all biological samples were considered for further analysis. The metabolites that passed our criteria were input into the software and the pathway enrichment analysis was run. The output of this algorithm marks a metabolic pathway if the input list of the metabolites suggests that the pathway associated with a specific pathway are present at levels that would not be expected by random chance.

Statistical Analysis. All experiments were repeated at least three times (three separate donors) and data was analyzed for significant variations ($p < 0.05$) using the Student's t-test and Dunnett's Multiple Comparison test.

1. Spoerl, E., Huhle, M. & Seiler, T. Induction of cross-links in corneal tissue. *Exp Eye Res.* **66**, 97–103, doi:10.1006/exer.1997.0410 (1998).
2. Spoerl, E., Schreiber, J., Hellmund, K., Seiler, T. & Knuschke, P. [Studies on the stabilization of the cornea in rabbits]. *Zeitschrift der DOG* **97**, 203–206 (2000).
3. Rahi, A., Davies, P., Ruben, M., Lobascher, D. & Menon, J. Keratoconus and coexisting atopic disease. *Br J Ophthalmol.* **61**, 761–764, doi:DOI 10.1136/bjo.61.12.761 (1977).
4. Gasset, A. R., Hinson, W. A. & Frias, J. L. Keratoconus and atopic diseases. *Ann Ophthalmol.* **10**, 991–994 (1978).

5. Bawazeer, A. M., Hodge, W. G. & Lorimer, B. Atopy and keratoconus: a multivariate analysis. *Br J Ophthalmol.* **84**, 834–836, doi:DOI 10.1136/Bjo.84.8.834 (2000).
6. Cullen, J. F. & Butler, H. G. Mongolism (Down's Syndrome) and Keratoconus. *Br J Ophthalmol.* **47**, 321–330 (1963).
7. Shapiro, M. B. & France, T. D. The ocular features of Down's syndrome. *Am J Ophthalmol.* **99**, 659–663 (1985).
8. Robertson, I. Keratoconus and the Ehlers-Danlos syndrome: a new aspect of keratoconus. *Med J Aust.* **1**, 571–573 (1975).
9. Woodward, E. G. & Morris, M. T. Joint hypermobility in keratoconus. *Ophthalmic Physiol Opt.* **10**, 360–362 (1990).
10. Pierse, D. & Eustace, P. Acute keratoconus in mongols. *Br J Ophthalmol.* **55**, 50–54 (1971).
11. Udar, N. *et al.* SOD1: a candidate gene for keratoconus. *Invest Ophthalm Vis Sci.* **47**, 3345–3351, doi:10.1167/iov.05-1500 (2006).
12. Nowak, D. M. & Gajecka, M. The genetics of keratoconus. *MEAJO.* **18**, 2–6, doi:10.4103/0974-9233.75876 (2011).
13. Halliwell, B. Oxidative stress and cancer: have we moved forward? *Biochem J.* **401**, 1–11, doi:DOI 10.1042/Bj20061131 (2007).
14. Valko, M. *et al.* Free radicals and antioxidants in normal physiological functions and human disease. *The international journal of biochemistry & cell biology* **39**, 44–84, doi:10.1016/j.biocel.2006.07.001 (2007).
15. Singh, N., Dhalla, A. K., Seneviratne, C. & Singal, P. K. Oxidative stress and heart failure. *Mol Cell Biochem.* **147**, 77–81 (1995).
16. Dean, O. M. *et al.* N-acetyl cysteine restores brain glutathione loss in combined 2-cyclohexene-1-one and d-amphetamine-treated rats: relevance to schizophrenia and bipolar disorder. *Neurosci Lett.* **499**, 149–153, doi:10.1016/j.neulet.2011.05.027 (2011).
17. Ramond, A. *et al.* Oxidative stress mediates cardiac infarction aggravation induced by intermittent hypoxia. *FCP.* **27**, 252–261, doi:10.1111/j.1472-8206.2011.01015.x (2011).
18. Kenney, M. C., Brown, D. J. & Rajeev, B. Everett Kinsey lecture. The elusive causes of keratoconus: a working hypothesis. *CLAO J.* **26**, 10–13 (2000).
19. Greiner, J. V., Kopp, S. J. & Glonek, T. Phosphorus nuclear magnetic resonance and ocular metabolism. *Surv Ophthalmol.* **30**, 189–202 (1985).
20. Risa, O. *et al.* Metabolic changes in rat lens after in vivo exposure to ultraviolet irradiation: measurements by high resolution MAS 1H NMR spectroscopy. *Invest Ophthalm Vis Sci.* **45**, 1916–1921 (2004).
21. Karamichos, D. *et al.* Novel *in vitro* model for keratoconus disease. *JFB.* **3**, 760–775, doi:10.3390/jfb3040760 (2012).
22. Locasale, J. W. *et al.* Metabolomics of human cerebrospinal fluid identifies signatures of malignant glioma. *Molecular & cellular proteomics: MCP.* **11**, M111014688, doi:10.1074/mcp.M111.014688 (2012).
23. Kelly, A. D. *et al.* Metabolomic profiling from formalin-fixed, paraffin-embedded tumor tissue using targeted LC/MS/MS: application in sarcoma. *PLoS One* **6**, e25357, doi:10.1371/journal.pone.0025357 (2011).
24. Yuan, M., Breitkopf, S. B., Yang, X. & Asara, J. M. A positive/negative ion-switching, targeted mass spectrometry-based metabolomics platform for bodily fluids, cells, and fresh and fixed tissue. *N prot.* **7**, 872–881, doi:10.1038/nprot.2012.024 (2012).
25. Webhofer, C. *et al.* Proteomic and metabolomic profiling reveals time-dependent changes in hippocampal metabolism upon paroxetine treatment and biomarker candidates. *J Psychiatr Res.* **47**, 289–298, doi:10.1016/j.jpsychires.2012.11.003 (2013).
26. Guo, X. *et al.* Morphologic characterization of organized extracellular matrix deposition by ascorbic acid-stimulated human corneal fibroblasts. *Invest Ophthalm Vis Sci.* **48**, 4050–4060, doi:10.1167/iov.06-1216 (2007).
27. Karamichos, D., Hutcheon, A. E. & Zieske, J. D. Transforming growth factor-beta3 regulates assembly of a non-fibroblastic matrix in a 3D corneal model. *JTERM* **5**, e228–238, doi:10.1002/term.429 (2011).
28. Karamichos, D. *et al.* TGF-beta3 stimulates stromal matrix assembly by human corneal keratocyte-like cells. *Invest Ophthalm Vis Sci.* **54**, 6612–6619, doi:10.1167/iov.13-12861 (2013).
29. Webhofer, C. *et al.* Proteomic and metabolomic profiling reveals time-dependent changes in hippocampal metabolism upon paroxetine treatment and biomarker candidates. *J Psychiatr Res.* **47**, 289–298, doi:DOI 10.1016/j.jpsychires.2012.11.003 (2013).
30. Xia, J. G., Psychogios, N., Young, N. & Wishart, D. S. MetaboAnalyst: a web server for metabolomic data analysis and interpretation. *Nucleic Acids Res.* **37**, W652–W660, doi:DOI 10.1093/Nar/Gkp356 (2009).
31. Klyce, S. D. Stromal lactate accumulation can account for corneal oedema osmotically following epithelial hypoxia in the rabbit. *J Physiol.* **321**, 49–64 (1981).
32. Doherty, J. R. & Cleveland, J. L. Targeting lactate metabolism for cancer therapeutics. *JCI.* **123**, 3685–3692, doi:10.1172/JCI69741 (2013).
33. Schutte, E., Schulz, I. & Reim, M. Lactate and pyruvate levels in the aqueous humor and in the cornea after cyclodiathermy. *Albrecht Von Graefes Arch Klin Exp Ophthalmol.* **185**, 325–330 (1972).
34. Li, G. B., Lee, P., Mori, N., Yamamoto, I. & Arai, T. Long term intensive exercise training leads to a higher plasma malate/lactate dehydrogenase (M/L) ratio and increased level of lipid mobilization in horses. *Vet Res Commun.* **36**, 149–155, doi:DOI 10.1007/s11259-012-9515-0 (2012).



35. Magalhaes, J. *et al.* Oxidative stress in humans during and after 4 hours of hypoxia at a simulated altitude of 5500 m. *Aviat Space Environ Med.* **75**, 16–22 (2004).
36. Zitka, O. *et al.* Redox status expressed as GSH:GSSG ratio as a marker for oxidative stress in paediatric tumour patients. *Oncol Lett.* **4**, 1247–1253, doi:10.3892/Ol.2012.931 (2012).
37. Chai, Y. C., Ashraf, S. S., Rokutan, K., Johnston, R. B., Jr. & Thomas, J. A. S-thiolation of individual human neutrophil proteins including actin by stimulation of the respiratory burst: evidence against a role for glutathione disulfide. *Arch Biochem Biophys.* **310**, 273–281, doi:10.1006/abbi.1994.1167 (1994).
38. Arnal, E., Peris-Martinez, C., Menezo, J. L., Johnsen-Soriano, S. & Romero, F. J. Oxidative stress in keratoconus? *Invest Ophthalmol Vis Sci.* **52**, 8592–8597, doi:10.1167/iovs.11-7732 (2011).
39. Fu, H. *et al.* Arginine depletion as a mechanism for the immune privilege of corneal allografts. *Eur J Immunol.* **41**, 2997–3005, doi:10.1002/eji.201141683 (2011).
40. Nguyen, T. T. & Bonanno, J. A. Lactate-H⁺ transport is a significant component of the in vivo corneal endothelial pump. *Invest Ophthalmol Vis Sci.* **53**, 2020–2029, doi:10.1167/iovs.12-9475 (2012).
41. Paracha, U. Z. *et al.* Oxidative stress and hepatitis C virus. *Virology J.* **10**, 251, doi:10.1186/1743-422X-10-251 (2013).
42. Seaver, L. C. & Imlay, J. A. Are respiratory enzymes the primary sources of intracellular hydrogen peroxide? *JBC.* **279**, 48742–48750, doi:10.1074/jbc.M408754200 (2004).
43. Cadenas, E. Mitochondrial free radical production and cell signaling. *Mol Aspects Med.* **25**, 17–26, doi:10.1016/j.mam.2004.02.005 (2004).
44. Pollack, M. & Leeuwenburgh, C. Apoptosis and aging: role of the mitochondria. *Journals Gerontol A Biol Sci Med Sci.* **56**, B475–482 (2001).
45. Lee, H. C. & Wei, Y. H. Mitochondrial biogenesis and mitochondrial DNA maintenance of mammalian cells under oxidative stress. *Int J Biochem Cell Bio.* **37**, 822–834, doi:10.1016/j.biocel.2004.09.010 (2005).
46. Mugge, A. *et al.* Chronic treatment with polyethylene-glycolated superoxide dismutase partially restores endothelium-dependent vascular relaxations in cholesterol-fed rabbits. *Circ Res.* **69**, 1293–1300 (1991).
47. Miller, F. J., Jr., Gutterman, D. D., Rios, C. D., Heistad, D. D. & Davidson, B. L. Superoxide production in vascular smooth muscle contributes to oxidative stress and impaired relaxation in atherosclerosis. *Circ Res.* **82**, 1298–1305 (1998).
48. Houstis, N., Rosen, E. D. & Lander, E. S. Reactive oxygen species have a causal role in multiple forms of insulin resistance. *Nature* **440**, 944–948, doi:10.1038/nature04634 (2006).
49. Chwa, M. *et al.* Hypersensitive response to oxidative stress in keratoconus corneal fibroblasts. *Invest Ophthalmol Vis Sci.* **49**, 4361–4369, doi:10.1167/iovs.08-1969 (2008).
50. Karicherla, P., Aras, S., Aiyar, A. & Hobden, J. A. Nona-D-arginine amide suppresses corneal cytokines in *Pseudomonas aeruginosa* keratitis. *Cornea.* **29**, 1308–1314, doi:10.1097/ICO.0b013e3181ca3a69 (2010).
51. Pompella, A., Visvikis, A., Paolicchi, A., De Tata, V. & Casini, A. F. The changing faces of glutathione, a cellular protagonist. *Biochem Pharmacol.* **66**, 1499–1503 (2003).
52. Gondhowiardjo, T. D. *et al.* Analysis of corneal aldehyde dehydrogenase patterns in pathologic corneas. *Cornea* **12**, 146–154 (1993).
53. Gondhowiardjo, T. D. & van Haeringen, N. J. Corneal aldehyde dehydrogenase, glutathione reductase, and glutathione S-transferase in pathologic corneas. *Cornea.* **12**, 310–314 (1993).
54. Buddi, R. *et al.* Evidence of oxidative stress in human corneal diseases. *J Histochem Cytochem.* **50**, 341–351 (2002).
55. Wenk, J. *et al.* UV-induced oxidative stress and photoaging. *Curr Probl Dermatol.* **29**, 83–94 (2001).
56. Abedinia, M., Pain, T., Algar, E. M. & Holmes, R. S. Bovine corneal aldehyde dehydrogenase: the major soluble corneal protein with a possible dual protective role for the eye. *Exp Eye Res.* **51**, 419–426 (1990).
57. Rao, N. A., Romero, J. L., Fernandez, M. A., Sevanian, A. & Marak, G. E., Jr. Role of free radicals in uveitis. *Surv Ophthalmol.* **32**, 209–213 (1987).
58. Brooker, R. J. *Genetics: Analysis and Principles*. 4th edn, (McGraw-Hill Science, 2011).
59. Devasagayam, T. P. *et al.* Free radicals and antioxidants in human health: current status and future prospects. *J Assoc Physicians India.* **52**, 794–804 (2004).

Acknowledgments

The authors thank Min Yuan and Susanne Breitkopf for technical help with mass spectrometry experiments. This work was partially supported by National Institutes of Health Grant 5R01EY023568 (D.K.), EY06000 (V.T.R.), Mass Lions Fund (V.T.R.), 2P01CA120964 (J.M.A.) and Dana-Farber/Harvard Cancer Center Support Grant 5P30CA006516 (J.M.A.).

Author contributions

All authors contributed extensively to the work presented in this paper. D.K. and J.D.Z. designed the experiments and prepared the manuscript, D.K. executed the in vitro experiments, A.E.K.H. contributed to the manuscript preparation, C.B.R. executed and analyzed the RT-PCR experiment, V.T.R. helped interpreting the RT-PCR data and contributed to the manuscript preparation, J.M.A. executed the metabolomics experiments and contributed to the manuscript preparation.

Additional information

Competing financial interests: The authors declare no competing financial interests.

How to cite this article: Karamichos, D. *et al.* In vitro model suggests oxidative stress involved in keratoconus disease. *Sci. Rep.* **4**, 4608; DOI:10.1038/srep04608 (2014).



This work is licensed under a Creative Commons Attribution-NonCommercial-NoDerivs 3.0 Unported License. The images in this article are included in the article's Creative Commons license, unless indicated otherwise in the image credit; if the image is not included under the Creative Commons license, users will need to obtain permission from the license holder in order to reproduce the image. To view a copy of this license, visit <http://creativecommons.org/licenses/by-nc-nd/3.0/>